[redacted] (No WT. issued)

ITR-1624

This document consists of 38 pages.

No. 157 of 190 copies, Series A

ENIWETOK PROVING GROUND

APRIL – AUGUST

1958

Operation

HARDTACK

Preliminary Report

Project 2.7

NUCLEAR RADIATION FROM A DETONATION AT VERY-HIGH ALTITUDE [redacted]

HEADQUARTERS FIELD COMMAND,
ARMED FORCES SPECIAL WEAPONS PROJECT
SANDIA BASE, ALBUQUERQUE, NEW MEXICO

Issuance Date: July 18, 1958

Defense Nuclear Agency
6801 Telegraph Road
Alexandria, Virginia 22310-3398

ISST

30 May 1996

MEMORANDUM FOR DEFENSE TECHNICAL INFORMATION CENTER
ATTENTION: OCD/Mr. Bill Bush

SUBJECT: Removal of AD-A995344 and Inclusion of ITR-1624

The Defense Nuclear Agency Security Office (OPSSI) **has declassified and approved for public release the following report:**

ITR-1624
Operation Hardtack, Preliminary Report
Project 2.7, Nuclear Radiation From A
Detonation at Very-High Altitude.
Issuance date: July 18, 1958.

This office does not have a record of DTIC ever receiving the above referenced report. However, an extracted version under AD-A995344 is currently being sold at NTIS.

We request the removal of the extracted version, (AD-A995344, ITR-1624(EX), since the original version is now declassified and approved for public release.

A copy of the original report (ITR-1624) is enclosed for entry into the DTIC system.

We would appreciate notification of your accession number.

Ardith Jarrett

Enclosure:
A/S

Ardith Jarrett
Chief, Technical Support

April 5, 1960

ADDENDA SHEET for ITR-1624

NUCLEAR RADIATION FROM A DETONATION AT VERY-HIGH ALTITUDE (OPERATION HARDTACK PRELIMINARY REPORT, PROJECT 2.7)

NOTE. The ITR-1624, with the changes shown below, is considered the final report of Hardtack Project 2.7—no WT report will be issued.

1. Page 5. Add to the end of the abstract the following paragraph:

A Monte Carlo calculation of the scattered neutron flux has been performed and the results indicate that in this experiment the contribution from scattered neutrons is negligible compared with the direct flux.

2. Page 13, line 4. Replace the three paragraphs beginning with "Numerical calculation . . ." and ending with the end of Chapter 1, with the following paragraph:

Numerical evaluation of K (E, t'), Equation 3, was carried out using the rocket panel atmosphere on an IBM 704 computer. These preshot results indicated that for the shot geometry the contribution of the scattered-in neutron signal was well within the expected instrumental errors. The preshot calculations of K (E, t') are not given in this report because they have been superseded by a more accurate Monte Carlo calculation. An outline of the Monte Carlo calculated routine is given and graphical results for K (E, t') will be presented in WT-1623, Neutron Flux from Very-High-Altitude Bursts, Project 2.6, Hardtack.

DISTRIBUTION

Identical to ITR-1624

USAEC TECHNICAL INFORMATION SERVICE EXTENSION, P. O. BOX 401, OAK RIDGE, TENNESSEE

[redacted]

ITR–1624

OPERATION HARDTACK—PROJECT 2.7

NUCLEAR RADIATION FROM A DETONATION AT VERY-HIGH ALTITUDE [redacted]

P. A. Caldwell, Project Officer
P. Alers — H. D. Holmgren
R. J. Drachman — C. A. Pearse
T. D. Hanscome — J. R. Pennick
R. C. Waddel

U. S. Naval Research Laboratory
Washington, D. C.

Ernest A. Pinson

Ernest A. Pinson, Col, USAF
Technical Director

K. D. Coleman

K. D. Coleman, Col, USAF
Commander, Task Unit 7.1.3

John A. Chiment

John A. Chiment, Maj, USA
Director, Program 2

[redacted]

[redacted]

[redacted]

[redacted] FOREWORD

This report presents the preliminary results of one of the projects participating in the military-effect programs of Operation Hardtack. Overall information about this and the other military-effect projects can be obtained from ITR-1660, the "Summary Report of the Commander, Task Unit 3." This technical summary includes: (1) tables listing each detonation with its yield, type, environment, meteorological conditions, etc.; (2) maps showing shot locations; (3) discussions of results by programs; (4) summaries of objectives, procedures, results, etc., for all projects; and (5) a listing of project reports for the military-effect programs.

[redacted]

ABSTRACT

The objective was to measure the neutron spectrum and total prompt gamma ray flux produced by the detonation of a nuclear device of low yield (approximately 2 kt) at an altitude of about 90,000 feet. This information was to be obtained by suitable detectors in the vicinity of the nuclear device and telemetered to the ground to be recorded and subsequently analyzed.

The theory and instrumentation for measurement of neutron spectrum and total prompt-gamma-ray flux from a nuclear device detonated at an altitude of 85,000 feet is described.

Measurement of neutron time of flight with a Li^6I scintillator-photodiode detector, with a similar LiI detector for gamma-ray correction of the Li^6I detector, was planned. The measurement was to have extended to plus 120 msec. A CsI scintillation detector, whose output was integrated for the first 10 μsec after the zero time, and a KBr crystal, whose darkening was measured as a function of time for 120 msec after zero time, were to be used to detect gamma flux.

The detector outputs were to have been electronically encoded and recorded on a magnetic-tape recorder programmed to record for 120 msec after zero time, reduce its speed to $1/16$ of the recording speed, and continuously play back the data. The recorder output modulated a 70-kc voltage-controlled oscillator used in a standard frequency-modulated telemetering system. A ground station received and recorded the signal.

The Bendix command system shared by this project and Projects 1.10 and 8.2 failed, and no data was obtained.

[redacted]

PREFACE

Although the major portion of the experimental plan, design and fabrication of instruments was done by the Nucleonics Division personnel who participated in the field, the timely completion of the printed circuitry and the solution of circuit problems could not have occurred without the aid of the Instrumentation Branch of the Radiation Division of Naval Research Laboratory (NRL). In particular major contributions were made by G. Wall, P. Shifflett, W. Weedman, G. Brotzman, and L. Bowles.

CONTENTS

FIGURES

[redacted]

Chapter 1
INTRODUCTION

1.1 OBJECTIVES

The objective was to measure the neutron spectrum and total prompt gamma ray flux produced by the detonation of a nuclear device of low yield (approximately 2 kt) at an altitude of about 90,000 feet. This information was to be obtained by suitable detectors in the vicinity of the nuclear device and telemetered to the ground to be recorded and subsequently analyzed.

1.2 BACKGROUND

During Operation Teapot, neutron flux from a device detonated at 36,600 feet above mean sea level (Shot 10) was measured by means of threshold fission and activation detectors in canisters dropped from the delivery aircraft. Gamma rays were measured with dosimeter films, DT/60/PD service dosimeters, silver phosphate glass and chemical dosimeters. Several fission-threshold detectors with thresholds at 200 ev, 1,000 ev, 700 kev, and 1,500 kev were used. The differences in flux given by these detectors were plotted as a histogram (Reference 1). A rough picture of the spectrum was given. Threshold detectors do not permit a detailed analysis of the spectrums for reasons discussed in Reference 1. Time-of-flight methods can give good energy-spectrum measurements if the geometry is good (neutrons scattered into the detector are excluded or negligible) and if the time duration of neutron production is short, compared to the mean time of flight.

At the altitude planned for the very-high-altitude burst (Shot Yucca), the air density is approximately 1 percent of the air density at sea level. For this small density and for small ranges, the time-of-flight method for measurements of neutron-energy spectra becomes feasible. The neutron-threshold data from Shot 10 of Operation Teapot was used to calculate the conditions for the measurement.

Originally, it was planned to use a "real time" telemeter link, i.e., the telemeter would transmit the signal instantaneously. It was noted, however, that the blast data telemeters in the near canisters during Shot 10 of Operation Teapot were inoperative for a period in the order of seconds, caused by absorption of the telemetering signal by the intense gamma-ray ionization produced by the nuclear device. The theory of this attenuation was inadequate for the calculation of the attenuation in the very-high-altitude case. It was not possible to choose either operating frequency or transmitter power without detailed knowledge of the attenuation.

Therefore, measurements of attenuation were made in the X band range during Operation Redwing (Reference 2). Although the measurements were successful, they were made at only one frequency and one range. On the basis of the Redwing data, a real-time link might be successful. To enlarge the data and to field test telemeter technique, fur-

ther measurements were made during Operation Plumbbob (Reference 3). The Plumbbob results indicated that a real-time link would not be feasible for any reasonable frequency or transmitter power.

The plans for Shot Yucca then necessarily included means for data storage so that data transmission could take place after the ionization had cleared up.

1.3 THEORY

An attractive procedure for measuring the energy spectrum of a neutron source is the time-of-flight method. It has been extensively applied in the past to cyclotron-produced, pulsed neutron beams and mechanically chopped reactor beams. Since the neutrons resulting from a nuclear detonation are all emitted in a relatively short time, the method is adaptable here also; but a relatively long path length is necessary, since many of the fission neutrons are very energetic. In addition, the extremely high particle flux available makes possible a detector system that need not count individual events, even at large distances from the source.

Suppose the detector is a distance l from the neutron source, and at first let us neglect the influence of air surrounding the system. In this idealized case, since all the observed neutrons travel directly from source to detector, there is a simple relation between time of arrival of a neutron (t) and its energy (E):

$$t = l \left(\frac{M}{2E} \right)^{1/2} \tag{1}$$

Where: M = neutron mass

The detector records the number of neutrons reaching the detector per unit of time, $\eta(t)$. Then, if N(E) is the number of neutrons per unit of energy emitted, the following simple relationship holds, with E and t connected by Equation 1:

$$\eta(t) = N(E)\, E^{3/2} \left(\frac{2^{3/2}}{l M^{1/2}} \right) \tag{2}$$

In the present experiment, l = 834 meters. Some typical neutron delay times are as follows (initial γ rays arrive at t = 2.78 μsec):

E	t
10 Mev	19.0 μsec
4	30.1
2	42.6
1	60.2
40 kev	300

The interpretation of the actual experiment is, of course, complicated by two effects: interaction of neutrons with the air and variation of detector efficiency with energy. In

order to unfold the raw data and to present an energy spectrum for the emitted neutrons, further analysis is necessary.

A considerable amount of work has appeared in the literature on the so-called buildup factor. This relates the observed total neutron flux to that expected in good geometry, but does not suffice to calculate time-of-flight corrections. In other words, one must account for those neutrons of a given energy that are lost from the direct beam and do not reach the detector at the proper time, as well as those inscattered neutrons of higher energy that arrive late due to their longer path and falsely simulate lower energy neutrons.

Suppose that the distribution in arrival time of a group of neutrons of energy E, which has been scattered and has finally reached the detector can be calculated (an approximate method for doing this will be described below). The function $K(E, t')$ is defined as the number of such neutrons reaching the detector at time t' per emitted neutron of energy E and, hence, falsely simulating neutrons of energy

$$E' = \frac{Ml^2}{2t'^2}$$

The system efficiency factor, Q(E), which specifies the signal recorded per neutron of energy E, is defined next. Since Q(E) varies slowly with E, the energy degradation that the neutrons undergo during collision with the air can be neglected. This energy degradation is small for most of the neutrons, since the mean number of scatterings experienced by a neutron is small. If $A(E')$ is the attenuation of the direct beam of energy E', due to scattering, absorption, and inverse-square effects, and $I(t')$ is the recorded signal at t', then

$$N(E') = \frac{l\,M^{1/2}}{2^{3/2}\,E'^{3/2}\,Q(E')\,A(E')} \left[I(t') - \int_{E'}^{\infty} dE\; Q(E)\, K(E, t')\, N(E) \right]$$

This is an inhomogeneous integral equation for the desired quantity N(E), the source intensity per unit of energy. The integral represents the total effect of all inscattered neutrons of energy higher than E', hence capable of being confused with direct neutrons of energy E'.

The problem of data reduction from a high-altitude detonation then is reduced to: (1) an evaluation of the kernel $K(E, t')$, which represents geometrical and physical properties of the atmosphere and its interaction with neutrons of all energies; (2) a calculation of the quantity Q(E); and (3) solution of the foregoing integral equation.

Problem 3 seems most susceptible to a stepwise numerical procedure, beginning with the highest energy groups and working downward. Experimental values of $I(t')$ are inserted, and successively lower values of E' are reached.

Problem 2 is essentially solved by the work on detector, recorder, and electronic calibrations given elsewhere in this report.

A simple digital-computer program has been set up to calculate the kernel $K(E, t')$, assuming single scattering of the neutrons and, again, assuming no energy degradation due to scattering in the air. The validity of this assumption and its applicability in the present case might well be questioned, but as a temporary expedient it seemed worthwhile pursuing.

Since there is little change of velocity during collision, use can be made of the focal

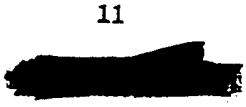

properties of ellipsoids of revolution. In Figure 1.1, the source and detector lie at the foci of a family of such ellipsoids such that

$$r_1 + r_2 = v t'$$

Where: $v = \sqrt{\frac{2E}{M}}$ = neutron velocity

In Formula 3 and the subsequent definitions the time of arrival, t', is measured in units

$$\bar{t} = \frac{l}{v}$$

for convenience.

$$K(E, t') = \frac{\alpha}{l} \int_{-b}^{1} dx \, \frac{\sigma(\cos\theta)\, n(Z)\, A_S(x)\, A_D(x)}{(t'^2 - x^2)} \tag{3}$$

Where: $b = 1$ or $\frac{2Z_0}{l t'}$

x = a variable of integration

α = detector area

$$\cos\theta = \frac{2 - t'^2 - x^2}{t'^2 - x^2}$$

$$Z = Z_0 + \frac{l t' x}{2}$$

$n(Z)$ = density of scatterers (oxygen and nitrogen nuclei) at altitude Z

$$Z = H + \frac{l}{2}(t'x - 1) = Z_0 + \frac{l t' x}{2}$$

H = shot altitude, $Z_0 = H - \frac{l}{2}$

$\sigma(\cos\theta)$ = differential scattering cross-section for neutrons.

$$A_S(x) = \exp\left[- \int_0^{r_1} \frac{dr_1}{\lambda(Z)} \right]; \text{ (attenuation factor)}$$

$$A_D(x) = \exp\left[- \int_0^{r_2} \frac{dr_2}{\lambda(Z)} \right]; \text{ (attenuation factor)}$$

[redacted]

$\lambda(Z)$ = mean free path for neutrons at altitude Z

$$= \frac{1}{\sigma_T\, n(Z)}$$

σ_T = total neutron cross-section in air.

Numerical evaluation of this kernel as a function of E and t' is underway, and the results will appear in a supplement to this report to be published at a later date.

Estimates have been made of the range of validity of the simple, one-scattering approximation proposed here. For an altitude of about 100,000 feet, the calculation should

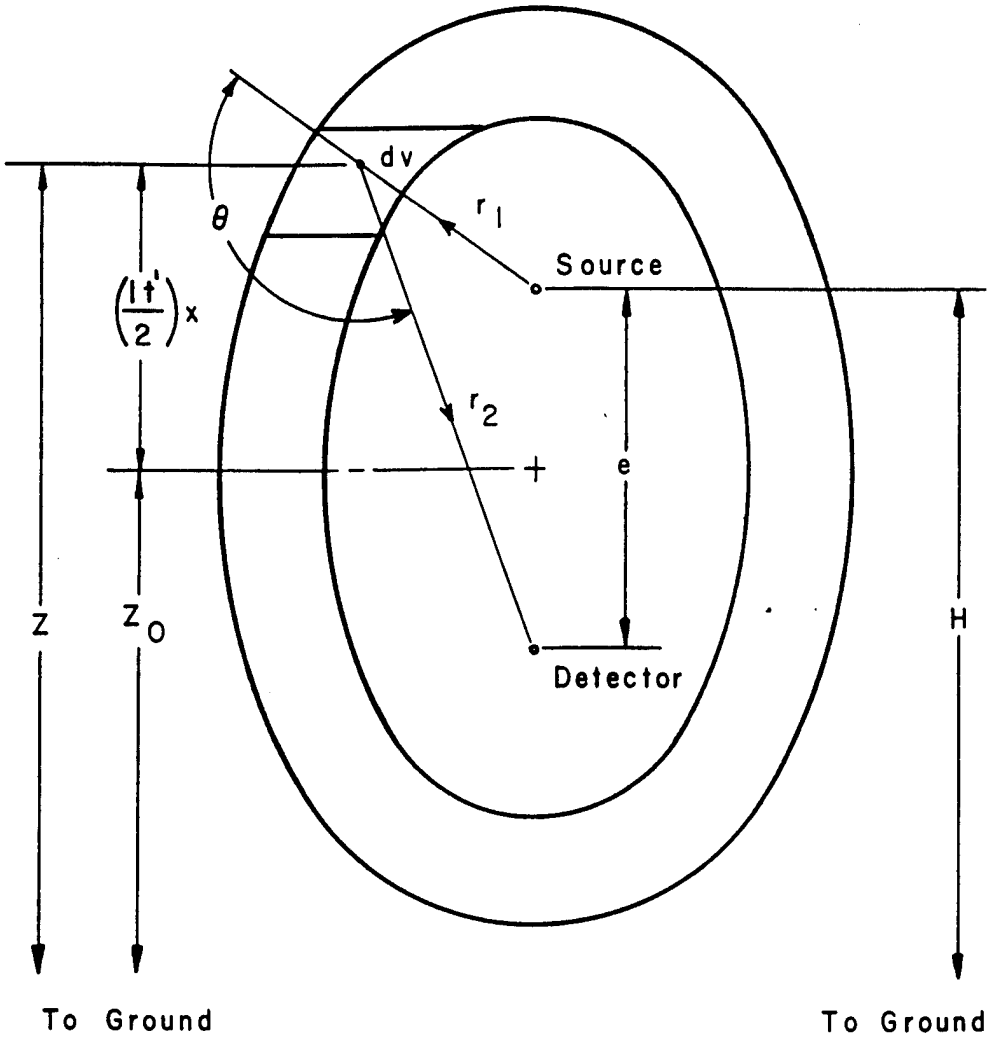

Figure 1.1 Coordinate system for scattering calculation.

be reliable out to $t' \geq 3\bar{t}$. This means, for example, that correction can be made for the effect of 10-Mev scattered neutrons at times corresponding to 1-Mev direct neutrons.

In an attempt to overcome the inherent limitations of the single scattering approximation, discussed above, constant liaison has been maintained with other agencies interested in this problem. The hope is to develop a "workable" Monte-Carlo type of machine program in evaluating K(E, t').

Chapter 2
OPERATIONS and INSTRUMENTATION

The instrumentation canisters and nuclear device were suspended from a large plastic balloon, launched at 1125:05, 28 April 1958, from the flight deck of the USS Boxer (CVS-21). Detonation occurred at 1440, 28 April 1958 at 85,000 feet at Latitude 12 degrees 37 minutes north and Longitude 163 degrees 01.5 minutes east, in the Eniwetok Proving Grounds. Command signals for operation of the equipment when floating altitude had been reached, as well as telemetering receiving and recording facilities, were provided by Project 1.10's "ground" station on the flight deck of the USS Boxer.

Project 2.7 instrumentation was contained in a pressurized aluminum vessel, 22 inches high and $8\frac{1}{4}$ inches in diameter, comprising the upper half of the Canister 5. The detectors were mounted in the top of the half canister, with the more massive components in the bottom. The lower half of Canister 5 and the other four canisters contained instrumentation used by Projects 8.2 and 1.10. Control and telemetering for Project 2.7 were accomplished by equipment mounted in the lower half of Canister 5, serving both Projects 2.7 and 1.10. At the time of detonation, Canister 5 was 2,750 feet from the nuclear device, or at an altitude of about 82,250 feet.

A time-of-flight neutron measurement was selected. Two scintillation detectors were used, one with a Li^6I crystal and one with a normal LiI crystal. The LiI and Li^6I crystals should respond to gamma rays in the same way. By comparison of their outputs, the neutron component can be isolated.

Two gamma-ray detectors were employed. The first used a CsI crystal as a scintillator, the second, a KBr crystal in which the darkening produced by gamma radiation was measured. The CsI detector channel was designed to measure the integral of the gamma radiation during the period from 0 to 10 μsec after detonation. The KBr detector is inherently an integrating device and would provide, at any time after detonation, the integral of the gamma radiation from 0 to t.

In the low-density air at 90,000 feet, it was believed that the five canisters might hang in a straight line, since there would probably be little wind shear in the 3,000 feet between the nuclear device and Canister 5. This would interpose the mass of the upper four canisters between the device and the detectors used by Project 2.7, introducing an unknown attenuation. To avoid this, Canister 5 was equipped with a small rocket (PET, manufactured by Atlantic Research Corporation, Alexandria, Virginia) producing 40 pounds of thrust for 1 second. This was to have been detonated at minus 2 seconds to produce a 0.5-g acceleration of the 80-pound canister. The resulting deflection of the canister would have been approximately 30 feet at zero time and continued to about 90 feet at plus 7 seconds.

The outputs of the four detectors were encoded electronically and recorded simultaneously on four parallel tracks of a magnetic-tape recorder having a recording time of about 120 msec. On completion of the recording operation, the tape speed was reduced to $\frac{1}{16}$ of the recording speed and the data played out, one channel at a time, into a standard Bendix 70-kc voltage-controlled oscillator and frequency-modulated transmitter lo-

cated in the lower half of Canister 5. This signal was received, demodulated, and recorded by the ground station.

2.1 DETECTORS

The detectors used in this experiment were designed to give a quantitative measurement of the absolute neutron spectrum and the gamma-ray dosage produced by the nuclear device. The expected performance of the device, from which preliminary calculations were made, was estimated from measurements made of an almost-identical device during Operation Teapot.

Since the shot was to take place at a very-high altitude (about 90,000 feet), it was known that the neutron spectrum could straight forwardly be obtained by a time-of-flight measurement. This involved the assumption that, for the purposes of instrument design, the effect of the atmosphere for neutron energies in excess of 0.1 Mev, is small at these altitudes. The gamma-ray flux was measured in two ways—the dosage in the initial pulse, integrated for 10 μsec, and the total dosage, integrated for 120 msec.

2.1.1 Description. The detector used to measure the neutron flux employed a scintillation crystal of enriched (95 percent) Li^6I and a 926 photodiode to measure the light output of the crystal. The Li^6 rendered the crystal sensitive to neutrons mainly through the $Li^6(n, \alpha)H^3$ reaction. In order to provide a suitable control for this crystal and, in particular, to observe its gamma response, a crystal of identical geometry composed of ordinary LiI was used as a second detector. Since 7.5 percent of normal lithium is Li^6, the output of this detector due to neutrons should be only 7.9 percent of that of the Li^6I. The difference in output of these two crystals, after a suitable correction for the presence of Li^6, can therefore be taken to be due solely to neutron activity.

The initial burst of gamma radiation was monitored by a cesium iodide crystal. In this case, the crystal was small (about 0.1 cc) and was taped directly to the face of a 926 phototube. The integral of the gamma dosage over the first 10 μsec was read from the output of this detector. In addition, the detector furnished a pulse to the associated electronic circuitry to initiate the time sequences necessary for the proper collection of data from all the detectors.

The fourth detector was used to determine the total gamma dosage measured over a period of 120 msec. This detector consisted of a crystal of potassium bromide treated so as to color under the action of gamma rays. The resulting change in light transmission was measured by means of a lamp and a small (1P42) photodiode. The sensitivity of the crystal was such that dosages ranging from 50 to 2,000 r were easily detectable.

2.1.2 Calibration. The calibration of the neutron detectors was for the purpose of establishing the relationship between the neutron flux passing through the detectors and the corresponding output currents of the photodiodes. Since it was necessary to calibrate the detectors over a considerable range of energies, the NRL 2 Mev Van de Graaff generator was used to produce monoergic neutrons from the following reactions:

$T(p, n)He^3$	(0.15, 0.25 and 0.36 Mev neutrons)
$D(d, n)He^3$	(4.25 Mev neutrons)
and $T(d, n)He^4$	(15.0 Mev neutrons)

A photomultiplier was used to observe individual events in the crystals, since the neutron fluxes available were too small to permit direct observation by a photodiode of the light

from the LiI. The photomultiplier produced a series of pulses, which were recorded with a 256-channel pulse-height analyzer.

Since the channel number of each event was proportional to the light output of the crystal for that event, a quantity $P(E_n)$, representing the total light output at a given neutron energy E_n, could be defined as:

$$P(E_n) = \sum_{j=1}^{256} j\, m_j$$

Where: j = channel number

m_j = number of counts in that channel

At higher neutron energies, reactions other than those listed above began to take place, namely $Li^6(n, dn)He^4$ and $Li^7(n, d)He^6$, as well as gamma activity arising from the inelastic scattering of neutrons on iodine. All of these processes contributed to the light output of the crystal and formed a continuous background, which increased with increasing energy.

The total neutron flux, N, was determined with the aid of a calibrated long counter, which subtended the same solid angle at the neutron source as the detector. The quantity $P(E_n)/N$ was then proportional to the average light output per unit of neutron flux.

It was then necessary to establish a relationship between the crystal's light output and the sensitivities of the photomultiplier and the photodiode. This determination was complicated by the fact that the spectral response of the two tubes was different. Therefore, a single crystal was used as a light source for both, and X rays from the NRL 21 Mev betatron were sufficiently intense to be used for excitation.

By measurement of the charge released by the photodiode when a high intensity betatron pulse was incident upon the crystal and comparison of it with that produced by the photomultiplier from a low-intensity pulse, it was possible to establish the desired relationship between the tube sensitivities.

The calibration formula could then be expressed:

$$Q_n^{PD}(E_n) = \frac{\gamma_{PM}}{\gamma_{PD}} \frac{[P(E_n)/N]}{p_\beta} Q_\beta^{PD}$$

The value $Q_n^{PD}(E_n)$ = average charge released by the photodiode per unit of neutron flux of energy E_n striking the crystal;

γ_{PM} and γ_{PD} = radiation dosages per burst at the low and high levels, respectively;

p_β = height of the pulse produced by the photomultiplier for a low-intensity betatron burst;

Q_β^{PD} = charge released by the photodiode for a high-intensity burst

The value $P(E_n)/N$ was defined above.

The curve shown in Figure 2.1 represents $Q_n^{PD}(E_n)$ as a function of energy for both Li^6I and the normal crystal, Li^NI. By use of the measured current outputs of the photo-

diodes in conjunction with these curves and conversion of the time-of-flight information to energy, it was thus possible to determine the neutron-energy spectrum.

The calibration of the gamma-ray detectors consisted of determining, in one case, the charge liberated by a photodiode due to the scintillations of a small crystal of cesium iodide (CsI) and, in the other case, the change in light transmission of a crystal of potassium bromide (KBr).

The CsI detector was calibrated by its exposure to a calibrated gamma-radiation field produced by a Co^{60} source. The output currents of the photodiode were measured with a vibrating-reed electrometer.

The CsI detectors were also exposed to $\frac{1}{4}$-μsec bursts of X rays from the NRL betatron. The charge produced by the photodiode as a result of an X ray burst striking the crystal was measured. From the known radiation dose in each burst, it was possible to obtain a value of the photodiode current for a given radiation rate. It was found that the calibration figure in coulombs per roentgen for the Co^{60} source was about 32 percent higher than that for the betatron. This can be understood when it is realized that a larger percentage of incident gamma energy is deposited in a small crystal when the energy is low. The X rays from the betatron were much more energetic than those from the Co^{60}. Since the energy spectrum of the Co^{60} more nearly approximated that expected from the device, the Co^{60} results were weighted more heavily.

The calibration figure for the tube and crystal used here was 0.7×10^{-10} coulombs/r.

The potassium bromide detector was also calibrated by exposure of the crystal to the Co^{60} source. The output current of the photodiode was measured as a function of time. From the known radiation rate and the photodiode current, the light transmission (defined as the ratio of photodiode currents before and after exposure) of the crystals could be expressed as a function of total gamma dose. The curve of transmission (I/I_0) as a function of dosage is given in Figure 2.2.

2.2 DATA ENCODER

A block diagram of this section of the equipment is shown in Figure 2.3. Each detector output controlled a coding circuit consisting of a converter, or variable-frequency pulse generator, followed by a single-stage binary scaler. Each such converter had a repetition rate range of about 1,000 to 100,000 pulses/sec, and could be adjusted to free run at any repetition rate in this range. A positive signal increased the frequency. Both LiI detector signals had logarithmic load resistors.

The so-called Log-R circuit is a nonlinear device for compressing a wide range of signal currents into a relatively narrow range of voltages, in a roughly logarithmic manner. It increases the probability that detector signals will not dirve the succeeding circuitry beyond its dynamic range. They are used in the Li^6I and LiI detector channels.

A simplified circuit of a Log-R is shown in Figure 2.4. As detector current I rises from zero, the only conducting path is through R_1, the other branches being opened by the reverse-biased diodes. The slope of the V-I relation is thus R until $V = V_1$, when VT1 becomes conducting. Further increase in I occurs with the function slope of R_1 and R_2 in parallel, V rising more slowly with I than before. Eventually, all diode paths are conducting and the function slope is that of R_1, R_2, R_3, and R_4 in parallel.

The design objectives were an approximate log characteristic for $0.001 \leq I \leq 100$ ma, circuit resistances large compared with diode resistances, bias voltages large compared to 1 volt, a rise time of less than 10 μsec, and a simple circuit. These objectives can

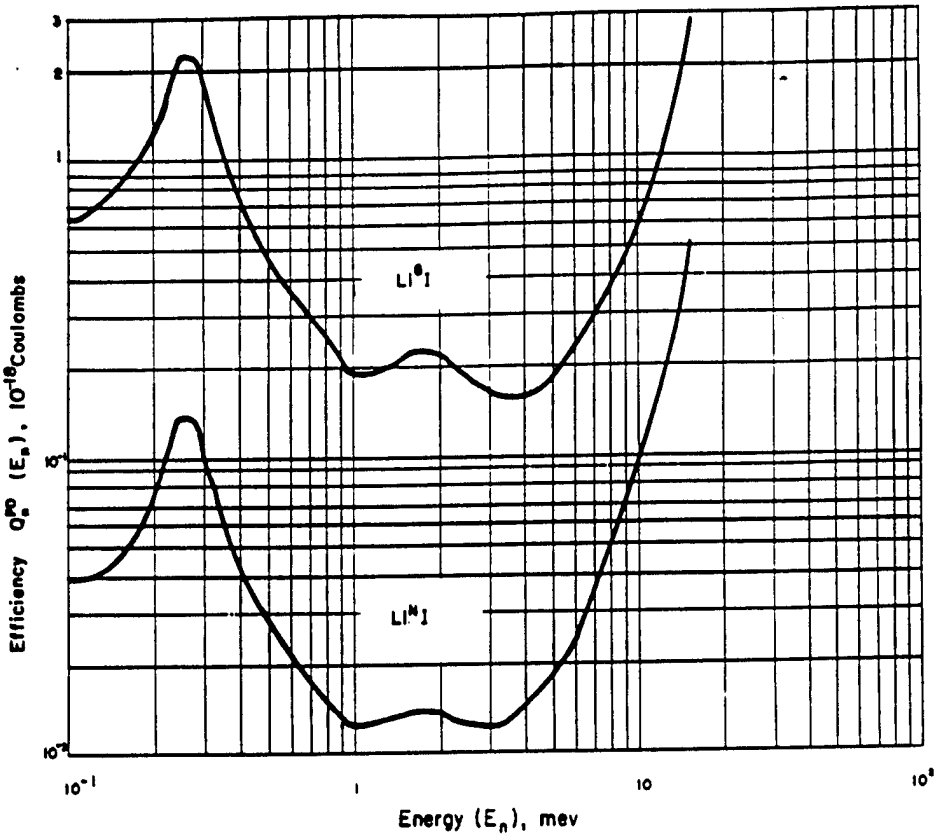

Figure 2.1 Efficiency of neutron detectors versus neutron energy.

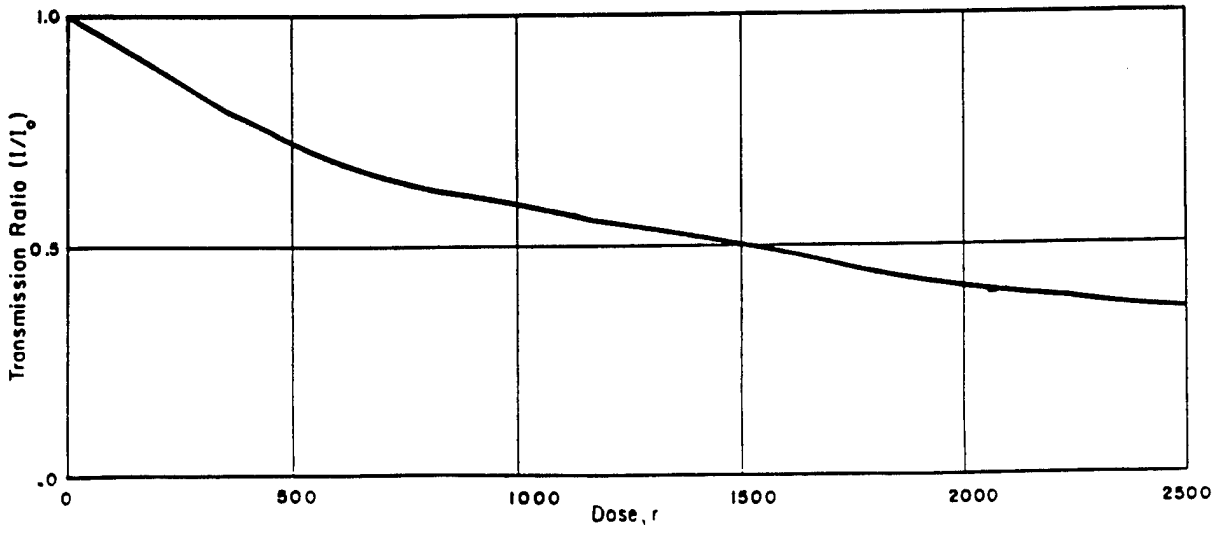

Figure 2.2 Transmission of KBr crystal versus gamma-ray dose.

[redacted]

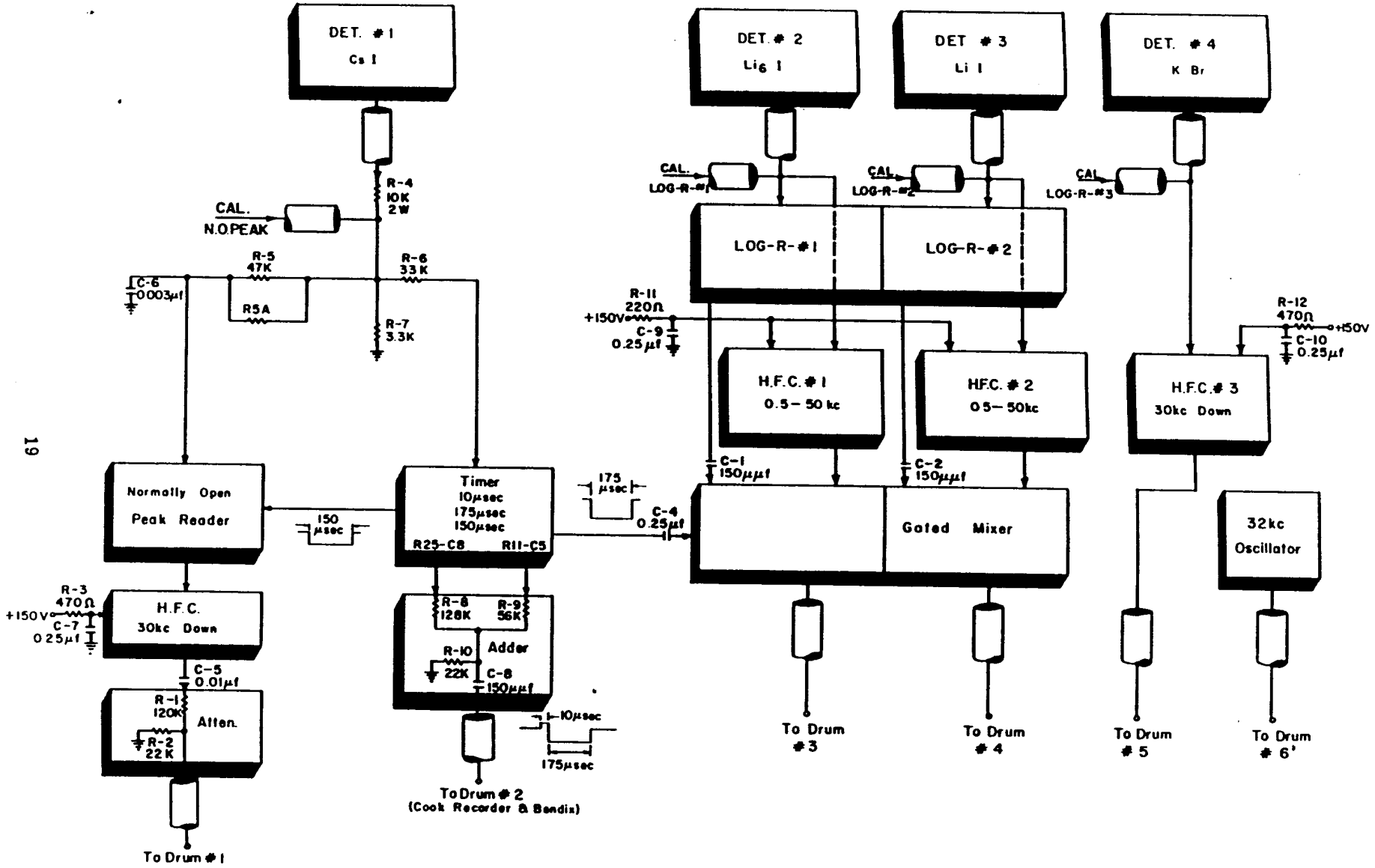

Figure 2.3 Block diagram of data encoder.

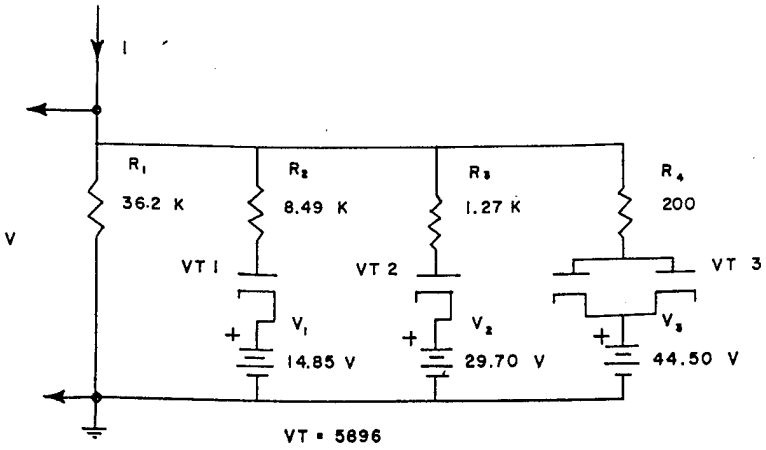

Figure 2.4 Schematic diagram of logarithmic-resistor.

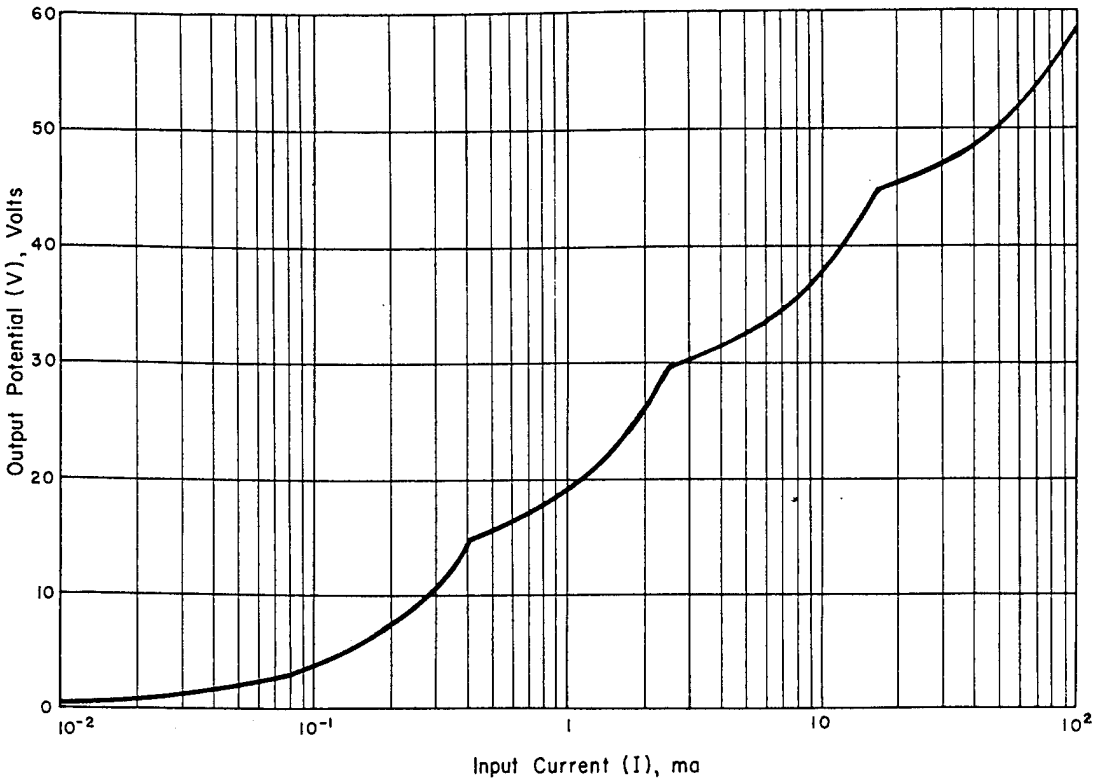

Figure 2.5 Calibration curve for typical logarithmic-resistor.

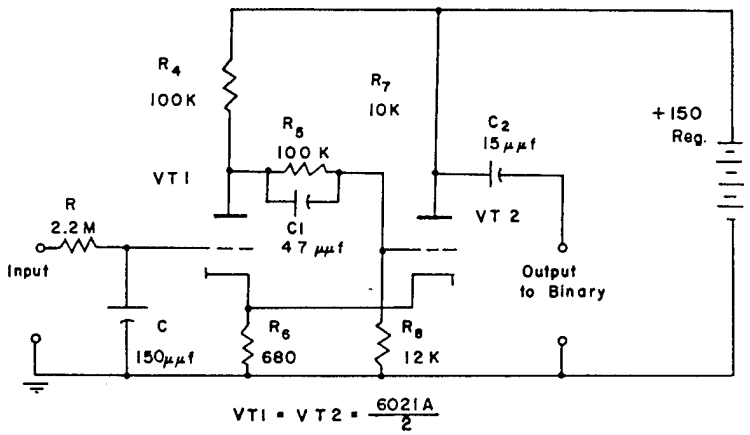

Figure 2.6 Schematic diagram of frequency converter (HFC).

be substantially achieved with the arrangement of Figure 2.4, if stable precision film resistors and stable bias batteries of low internal impedance are employed.

The values of R_2, R_3, and R_4 shown in Figure 2.4 include estimated diode incremental resistances of 290, 270, and 100 ohms, respectively.

Static calibration of the circuit was impossible, because of dissipation difficulties. Pulse calibration, which was tedious at best, gave results so near to the calculated values that calibration by calculation was employed. The relevant equations are given below:

$$V = R_1 I, \text{ for } 0 < V < V_1$$

$$V = V_1 + R_a I, \text{ for } V_1 < V < V_2, \text{ and}$$

R_a = parallel resistance of R_1 and R_2.

$$V = V_2 + R_b I, \text{ for } V_2 < V < V_3, \text{ and}$$

R_b = parallel resistance of R_1, R_2, and R_3.

$$V = V_3 + R_c I, \text{ for } V_3 < V < 60, \text{ and}$$

R_c = parallel resistance of R_1, R_2, R_3, and R_4.

Actually, only calculations for the points $V = 0$, $V = V_1$, $V = V_2$, $V = V_3$, and $V = 60$ need be made, since the circuit is linear between these points.

The calculated response of the two Log-R's employed is shown in Figure 2.5.

A converter (HFC) is used in all four detector channels to change relatively slowly varying direct current signals, unsuitable for magnetic recording, to frequency-modulated square-wave information.

The circuit of a typical converter, excluding the succeeding binary used for wave shaping, is shown in Figure 2.6.

Tubes VT1 and VT2 are in a direct-coupled regenerative loop. A signal voltage applied to the input terminals causes a changing current to flow into Capacitor C, raising the grid potential of VT1 in a substantially linear fashion. This tube is normally cut off, since VT2 tends to be heavily conducting. After a time the grid voltage of VT1 rises above cutoff and a rapid regenerative action forces VT1 to conduction and VT2 to non-conduction. The relatively large plate-load resistor (R_4 = 100k) for VT1 causes the bias current now flowing in R_8 to be smaller than before. The resulting low bias on VT1 causes the grid of that tube to be positive with respect to its cathode. A rapid partial discharge of capacitor C occurs and the tubes then revert to their initial conduction states. The action then repeats, generating a sawtooth wave across C. The frequency tends to be proportional to signal voltage. Short positive pulses are taken from the plate of VT2 for triggering a wave-shaping binary.

A typical calibration is shown in Figure 2.7. A small current is ordinarily fed to Capacitor C from the plate supply to maintain a standby oscillation during no-signal conditions.

Resistor R_8 is varied to adjust the response to a desired range. Regulated supplies and stable components are essential.

The CsI detector (Detector 1), in addition to its gamma-ray-measuring function, also provided a trigger pulse, which initiated a timing sequence. The CsI detector gate pulse and the LiI gate pulse (See Figure 2.3) generated here are added and recorded on tape

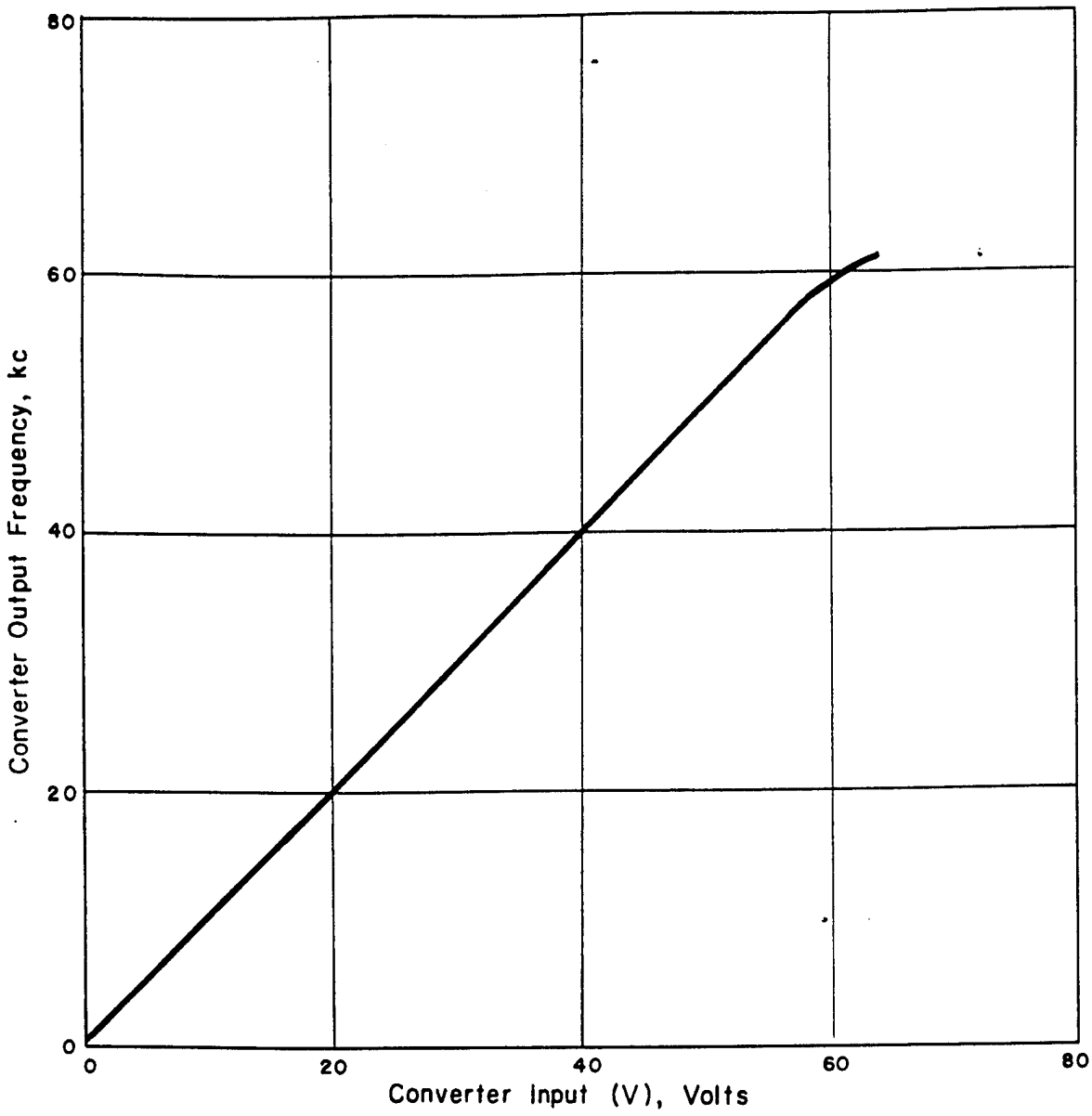

Figure 2.7 Output frequency versus input voltage for typical HFC.

Channel 1 to incorporate the actual gate times in the telemetered signal. This signal also went to the tape recorder to initiate its timing sequence and to the Project 1.10 equipment to provide them with a zero-time mark.

To accomplish the gamma-ray measurement, the CsI detector output was integrated in an RC circuit with a time constant long compared to the prompt-gamma-ray pulse and the resulting voltage used to actuate a peak-measuring circuit. The input to the normally open peak-measuring circuit was gated off at 10 μsec after gamma-ray arrival by a pulse generated by the gamma-ray pulse itself, so that the voltage held in the peak-measuring circuit was the value of the integrated detector current at 10 μsec. The negative output from the peak measuring circuit controlled a converter set to free run at 30 kc such that

an increase in the gamma-ray integral decreased the frequency. This signal was recorded on Channel 5 of the tape.

The KBr crystal was illuminated by a 12-volt incandescent light and its transmission was measured by a photocell whose output current controlled a converter free running at 30 kc such that the frequency decreased as the transmission of the crystal decreased. This signal was recorded on Channel 4 of the recorder.

For the two LiI detectors, the output of the corresponding converter was recorded on the tape, except for a 150-μsec interval beginning 10 μsec after gamma-ray arrival at the canister, when the magnitude of the detector current was recorded directly on the tape. This was necessitated by the inability of the recorder system to record pulses short enough to resolve the rapid variations of detector current expected during the early part of the neutron pulse. To accomplish this, both the converter output and LiI detector output were brought to a gated mixer. The detector output was taken to Input 1 of the gate of mixer through a high-pass filter to attenuate the slowly changing components of the detector-output current. The converter output was taken to Input 2. (See Figure 2.3.) Input 2 was gated off from plus 10 μsec to plus 160 μsec, relative to gamma-ray arrival time, and mixed with Input 1. The result of all this is that the output of the gated mixer consists of direct detector output when it is changing rapidly and converter output when it is changing slowly. Both the Li^6I and LiI detectors were treated in this way and recorded on Channels 3 and 2, respectively, of the tape.

The sixth channel of the tape was used to record the output of a 32-kc crystal-controlled oscillator, providing an internal time standard.

2.3 MAGNETIC-TAPE RECORDER

Instrumentation applications of this kind are faced with the problems of loss of reliable telemetry data transmission because of ionization of the atmosphere, limitation of the data channels available, and the inadequate high-frequency response available with standard RDB voltage-controlled subcarrier oscillators. The purpose of the magnetic recording system was to overcome these problems by providing data storage for six channels of information, time delay between the collection of data and the transmission of data, and reducing the frequency components of the data to, in effect, extend the frequency response of the voltage-controlled subcarrier oscillator.

The magnetic recording system consisted of a two-speed recorder with the electronic components required for recording, erasing, timing, and playback. A block diagram is shown in Figure 2.8. The inputs to the recording system were supplied by encoders and consisted of:

Channel 1. A pulse input positive for 10 μsec, negative for 150 μsec and 7 volts amplitude in each direction.

Channel 2. The output of a converter binary, which had a no-signal frequency of 500-cycles, square wave, and a full-signal frequency of 50 kc, square wave, with a level of 7 volts, peak to peak.

Channel 3. Same as Channel 2, except from a different converter binary.

Channel 4. The output of a converter binary with a zero input frequency of 30 kc and a full signal frequency of 500 cycles.

Channel 5. The output of a pulse-controlled oscillator that had a zero-input frequency of 30 kc and a full-signal frequency output of 500 cycles.

Channel 6. The output of a 32-kc crystal-controlled oscillator used to determine the exact speed-reduction ratio between record and playback, as well as an accurate time base for evaluation of the data.

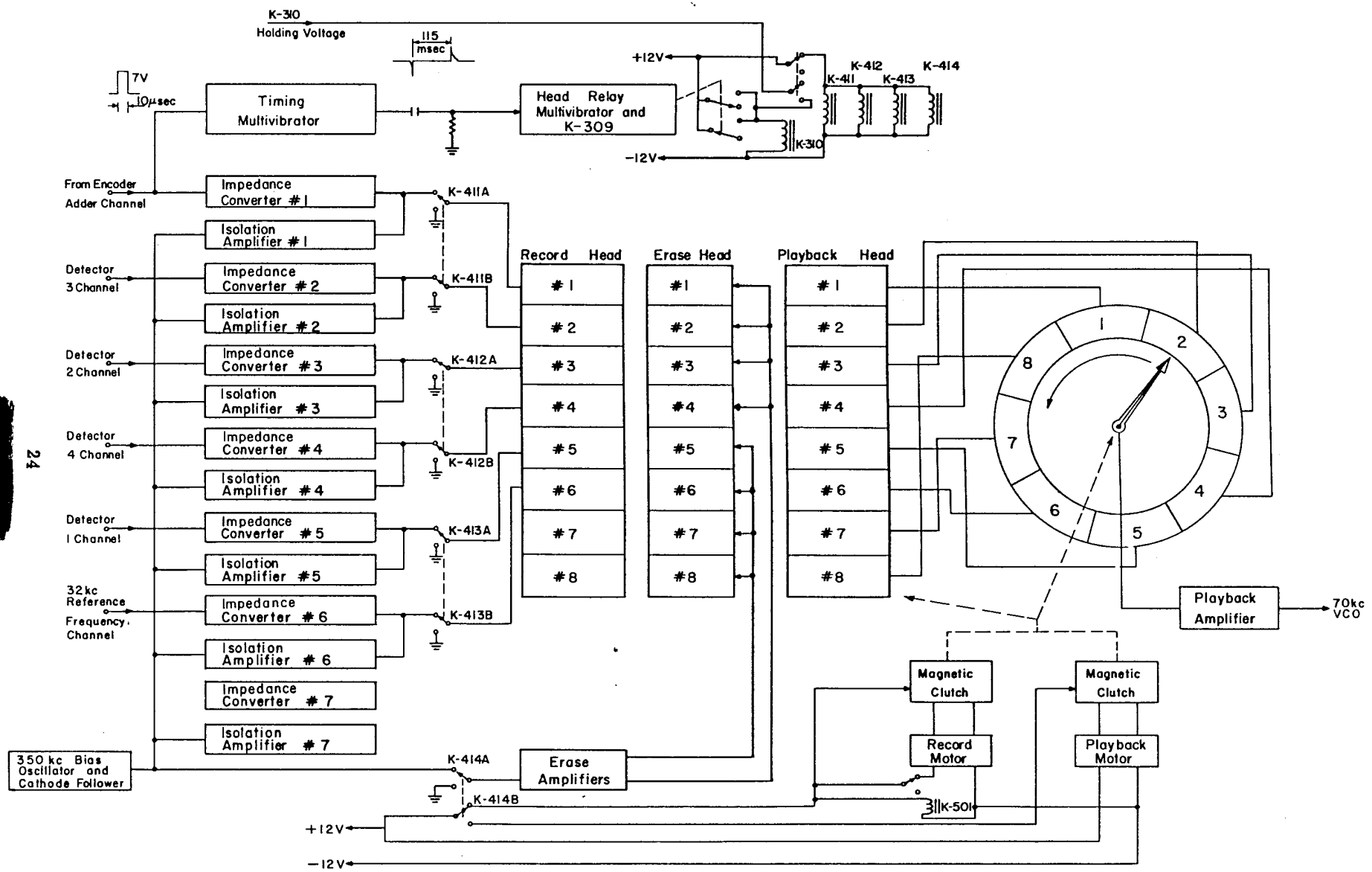

Figure 2.8 Block diagram of magnetic-tape recorder.

The inputs were applied directly to the impedance converter, which provided the necessary amplification and frequency pre-emphasis. The output of the impedance converter was mixed with the output of the isolation amplifier before being applied to the recording head. The recorder was always in the record mode when the system was turned on, and the data that was recorded was played back and erased before new data was recorded.

The input to Channel 1 was also applied to the input of a monostable multivibrator. This multivibrator was used to provide a positive pulse, delayed by 120 msec from the arrival of the 10-μsec pulse. The delayed positive pulse was applied to another multivibrator, which performed the function of shifting the recorder to the playback speed of $3\frac{3}{4}$ in/sec, turning the erase drive off, and removing the recording signal by grounding the recorder heads.

The playback head was connected to the playback amplifier through a commutator, which provided signal switching, to enable the playback amplifier to play back each channel of data twice. The commutator drive was connected to the recorder capstan drive to insure proper speed relationship in both record and playback modes. The playback amplifier provided the necessary gain to modulate the 70-kc voltage-controlled oscillator ± 15 percent. The frequency response of the playback amplifier was selected to provide the best operation from 50 cycles to 4 kc with a maximum signal-to-noise ratio being the prime consideration.

The erase amplifiers were necessary to erase the signals recorded prior to the arrival of the desired signals. The erase was turned off after the desired signals had been recorded. The length of recording time was 120 msec after the arrival of the gamma pulse.

2.3.1 Recording Electronics. Impedance Converters: The unit contained seven impedance converters. This application required the use of six converters, the seventh being used as a spare in the event of a failure of one of the active impedance converters.

The impedance-converter circuit consisted of a dual triode connected in parallel to obtain a low plate resistance to provide maximum power delivery into the low-impedance record head. The stage was designed to provide a constant recording head current with a constant input voltage for frequencies between 500 cycles and 50 kc. The grid input network was designed to provide a 6 decibel/octave roll off from 100 cycles to 7 kc, with 7 kc, being down 21 decibel, and rising 6 decibel/octave from 10 kc to 50 kc, with 50 kc down 7 decibel with respect to 100 cycles. The current-delivering capability of the impedance converter was 1 ma at 10 kc maximum.

Isolation Amplifiers: The unit contained seven isolation amplifiers and, as with the impedance converters, only six were used, with the seventh as a spare. The isolation amplifiers provided bias current to the record head. The circuit consisted of a dual triode connected in parallel to obtain the current-delivering capabilities to deliver 10 ma, at 350 kc, into the record head. The voltage gain of the network was 2.3, with primary design consideration being current delivered into a low-impedance load.

Bias Oscillator: The bias oscillator network was comprised of a twin T oscillator driving a cathode follower. The twin T oscillator circuit was selected for its simplicity and frequency stability over temperature and voltage changes. The cathode follower performed the function of a buffer and of matching impedances. The cathode follower drove all isolation amplifiers in parallel, representing a load of 10,000 ohms.

2.3.2 Timing Electronics. Timing Multivibrator: This provided the proper length of recording cycle. The monostable multivibrator had a negative output pulse 85 volts peak amplitude and a duration of 115 msec. The multivibrator was triggered by a 10-μsec

pulse, 7 volts peak amplitude, created by the arrival of the gamma pulse. The output of the timing multivibrator was differentiated and applied to the grid of the head-switching-relay network.

Head-Switching Assembly: The assembly consisted of a monostable multivibrator with a relay as plate load for the "on" plate, controlling Relay K-310, which controlled the state of Relays K-411, K-412, K-413, and K-414. The plate Relay K-309 was energized with the turn on of the system and remained energized until the arrival of a positive pulse from the timing multivibrator. Relay K-309 received plus 12 volts through the normally closed contacts of K-309 and, in turn, controlled the plus 12 voltage applied through K-310 normally closed contacts to Relays K-411, K-412, K-413, and K-414. Upon arrival of the positive pulse from the timing multivibrator, the head switching relay multivibrator changed state, de-energizing relay K-309, energizing K-310, and de-energizing Relays K-411, K-412, K-413, and K-414.

Relays K-411, K-412, and K-413 were the head-switching relays. When they were energized, the output of the impedance converter was applied to the record head; when de-energized the recording heads were grounded. Relay K-414 controlled the tape speed, and when energized, the magnetic clutch from the record motor was energized, connecting the record motor to the capstan. When Relay K-414 was de-energized, the clutch for playback was activated, and the playback motor was connected to the capstan. Relay K-501 controlled the record drive motor and turned it off in the playback mode.

Relay K-414 also controlled the 350-kc drive to the erase amplifier. When K-414 was de-energized, K-414 grounded the input to the erase amplifier.

Relay K-310 obtained plus 12 volts of holding voltage from the encoder network, and when it was applied the magnetic recording system went through one cycle, after the arrival of the 10-μsec pulse from the adder channel. If this voltage was not present, the system would not shift down into the playback mode.

2.3.3 Erase Electronics. Erase Amplifiers: The erase amplifier consisted of a drive amplifier and two push-pull amplifier networks. The drive amplifier was a single-triode amplifier with gain sufficient to provide 350 kc drive voltage to the power amplifiers. The power amplifiers were operated Class AB_1, and were capable of providing 10 watts into a load impedance of 10,000 ohms. The erase head was composed of eight erase tracks, each track having an impedance of 10,000 ohms, so when connected in series paralleled with three other tracks, an impedance of 10,000 ohms was obtained. Each push-pull network drove four erase tracks, each track having a power input of 2.5 watts. Each network had two adjustable controllers, one to provide alternating current balance, the other to provide the direct current balance. The direct current balance was critical, because there would be direct current in the erase windings and a direct current unbalance of 4 ma would erase the tape after the drive signals had been removed. The alternating current balance was necessary to obtain low distortion in the 350-kc signal. If distortion was present, it would create a direct current bias of the tape. The result of direct current bias on the tape could be serious second harmonic distortion of the recorded signal.

Transport: The transport was driven by two "globe" permanent-magnet, governor-controlled, motors. The governors were centrifugal and required arc suppressors to prevent contact arcing from getting into the power line. The record motors turned at 2350 rmp and the playback motor at 152 rpm. Attached to each motor were magnetic clutches gear-linked to a pulley that, in turn, drove the capstan at either the high or low speed, depending on the position of relay K-414.

The record head was a Brush-Clevite magnetic head. This head contained eight

tracks with each track having an inductance of 4.5 mh. An impedance converter and one isolation amplifier drove each track.

The erase head was a J. B. Rea magnetic erase head and, like the record head, consisted of eight tracks, each track having an inductance of 4 mh. The erase head was connected as a plate load for the erase amplifiers, with each track dissipating 2.5 watts of 350 kc signal.

The playback head is J. B. Rea high-inductance, narrow-gap-width playback head. The playback head had an inductance of 125 mh, and a gap width of 0.0001 inch.

The recording medium was magnetic tape $1\frac{1}{8}$ inches wide, 0.005 inch thick, produced by Reeves Sound Craft. This tape was selected for its resistance to wear and imperviousness to high temperatures.

Playback: The signal-switching commutator consisted of eight segments and a wiper segment. The purpose of the commutator was to play back each track of the record sequentially. The commutator wiper was connected mechanically to the recorder capstan drive through a 2-to-1 gear train. The gear reduction allowed each track to be played through twice before stepping to the next track. The stepping sequence was counterclockwise, playing back Channels 8 through 1, in that order.

The playback amplifier was a four-stage pentode amplifier with an open loop gain of 40,000 and a closed loop gain of 4,000. The primary response criterion was chosen to be a high signal-to-noise ratio at the high frequencies. The overall signal-to-noise ratio, from record to playback, was 18 to 20 decibels, with a recorded signal of 50 kc and having square wave form.

In operation, a frequency reduction of 16 to 1 resulted from the speed change from record to playback. (A recorded frequency spectrum of 500 cycles to 50 kc would result in a playback frequency spectrum of 30 to 3,000 cycles.) The playback-frequency spectrum was well within the frequency capabilities of the ground-station frequency modulation discriminator and recording oscillograph.

The overall frequency response is shown in Figure 2.9 and the frequency response of the record head, tape, and playback head is shown in Figure 2.10. These response curves indicate the effects of the high and low frequency pre-emphasis in the impedance converters.

2.4 CALIBRATION

This section describes the calibration of that portion of the instrumentation between the detectors and the magnetic-tape-recording amplifiers.

2.4.1 Detector 1 (CsI). Figure 2.11 indicates the procedure. The pulse generator delivered a pulse of amplitude V and duration t to the gamma-integrating network in the canister. Since duration t was small compared to the network time constant, the charge delivered was $g = Vt/R_s$ coulombs. The resulting high-frequency converter output was recorded on the tape at high speed, together with the output of the precision 32-kc oscillator. The tape was played back at low speed, and the reduced converter and oscillator frequencies were measured with a counter. The tape-speed-reduction factor was determined from the oscillator data and properly applied to the observed converter frequency to deduce the actual converter frequency associated with the input charge g. The relation is shown in Figure 2.12.

2.4.2 Detector 2 (Li^6I). The current input-voltage output characteristic of the Log-R was determined by calculation, employing the known component values and bias voltages.

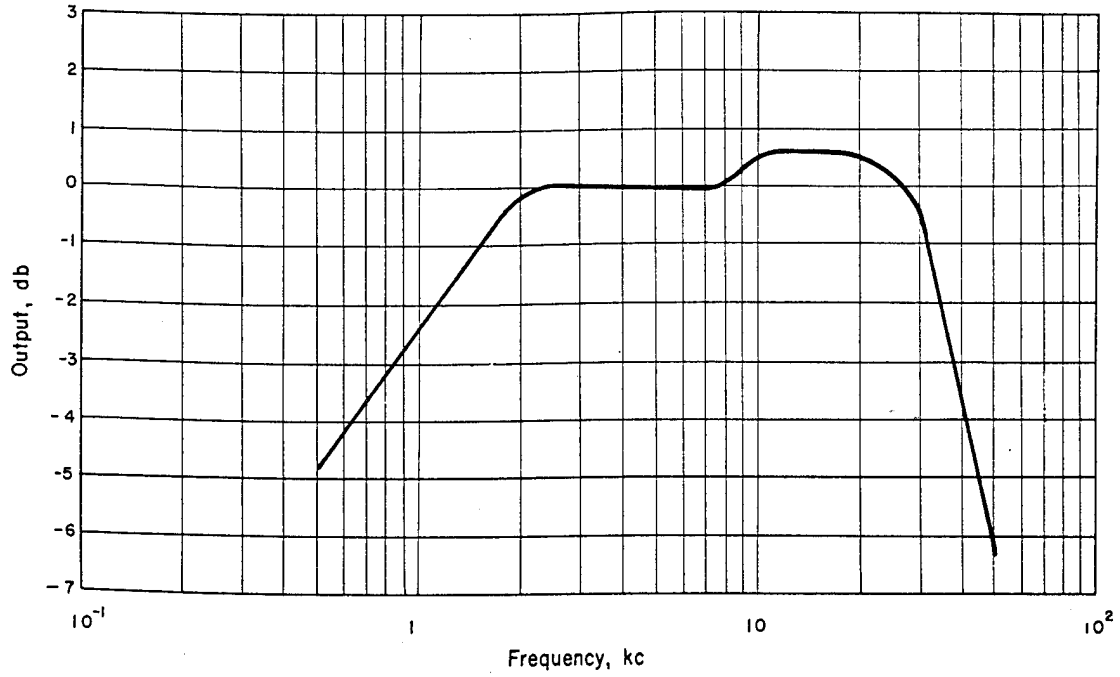

Figure 2.9 Overall frequency response of magnetic-tape recorder.

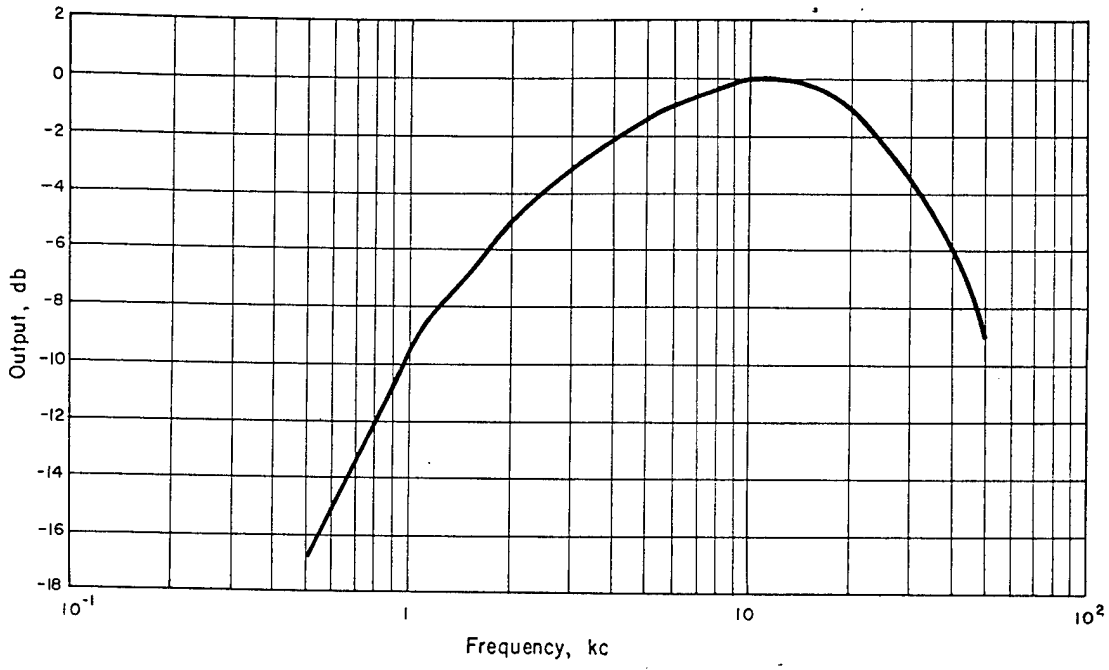

Figure 2.10 Frequency response of record head.

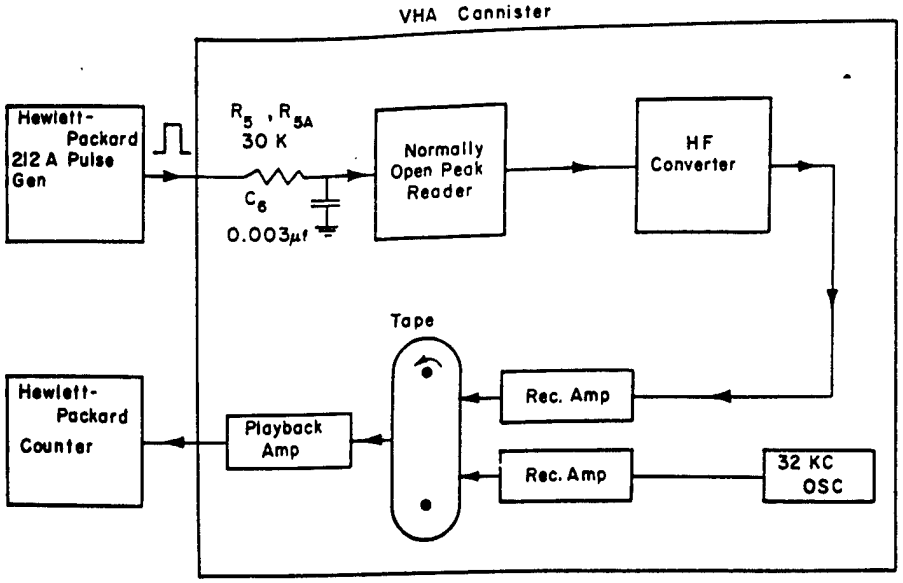

Figure 2.11 Detector 1 channel calibration setup.

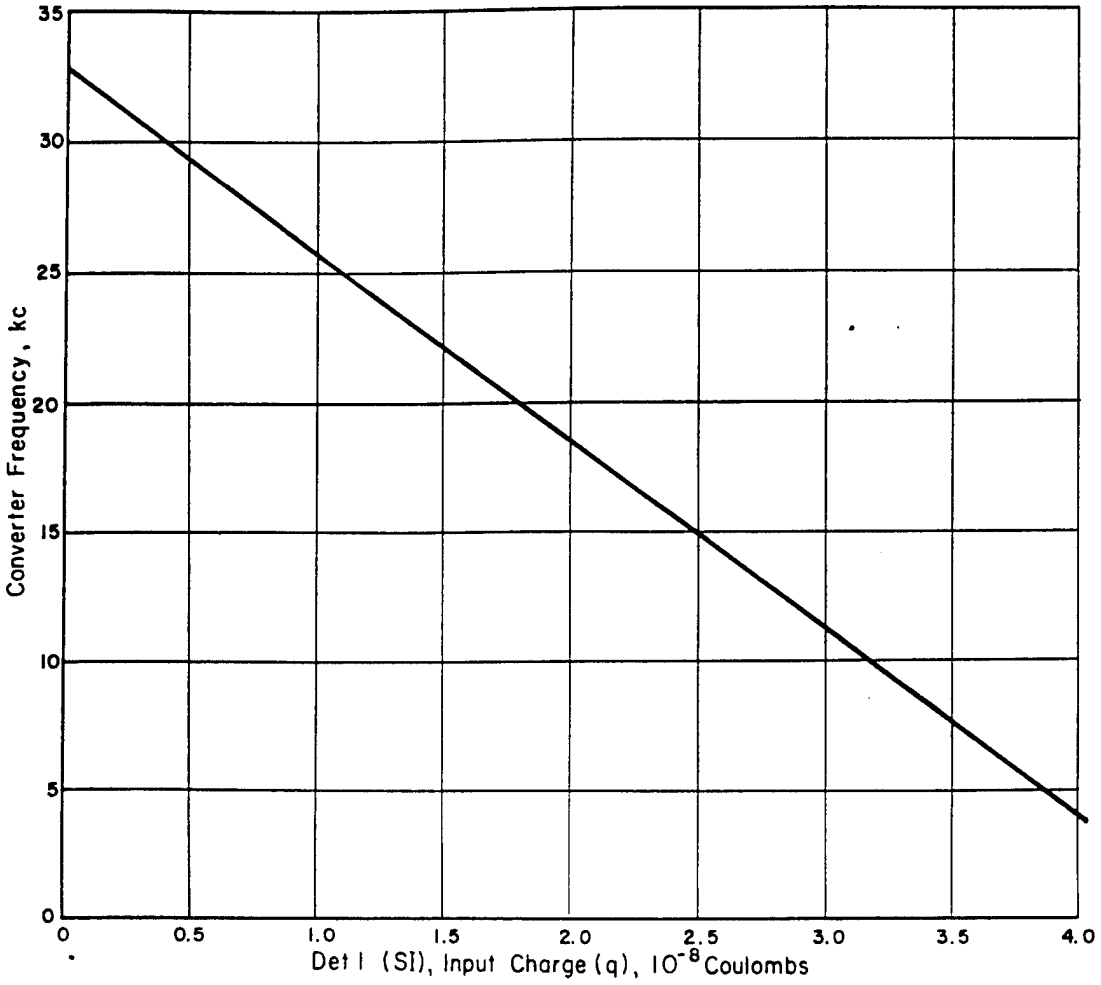

Figure 2.12 Detector 1 channel calibration curve.

The voltage input-frequency output characteristic of the high-frequency converter was determined by static measurements, using a direct current voltage source, a precise voltmeter, and a counter.

The complete current input-frequency output characteristic desired can be deduced from the data then available. It is shown in Figure 2.13.

2.4.3 Detector 3 (LiI). The procedure was the same as for Detector 2 Channel. The data is shown in Figure 2.14.

2.4.4 Detector 4 (KBr). The procedure here was to introduce measured currents, from a high-voltage, high-resistance source, to the proper detector lead, and then to measure the associated converter frequencies with a counter. The data is shown in Figure 2.15.

In addition to the preflight calibration discussed above, provisions were made to simulate signal inputs to the data encoder at minus 2 minutes. This was done with a condenser-thyratron single-tube pulser fired by command from the ground. This system provided pulses to all data channels and initiated the timing sequence, so that any deviation from the preflight condition could be detected.

2.5 COMMAND AND PROGRAMMING SYSTEM

The in-flight operation of the canister depended on five commands. The first four consisted of relay closures in the Project 1.10 equipment, initiated by the command transmitter in the ground station. The fifth was the arrival of the gamma-ray pulse at the canister.

2.5.1 Minus 7 Minutes. This command signal supplied internal battery power to all equipment in canisters, producing "ready" condition. The tape-recorder was recording, playing back, and erasing continuously. This provided a preliminary check on the operation of the equipment, since the free-running rate of the converters was being transmitted to the ground station.

2.5.2 Minus 2 Minutes. This command signal initiated the in-flight calibration sequence and provided the arming voltage required to hold the tape recorder in the playback mode. This command was maintained for 45 seconds, the period required to play back all eight channels on the tape. Its release restored the system to the "ready" condition.

2.5.3 Minus 10 Seconds. Up to this time, the system was reversible and could be reset by turning off the minus-7-minute command. However, the minus-10-second command produced some irreversible changes, which were required to reduce power drain during the playback period and to protect the system from shock-induced relay closures.

2.5.4 Minus 2 Seconds. This signal fired displacement rocket and supplied arming voltage to tape recover.

2.5.5 Gamma-Ray Pulse. Initiated timing sequence in tape recorder, causing the

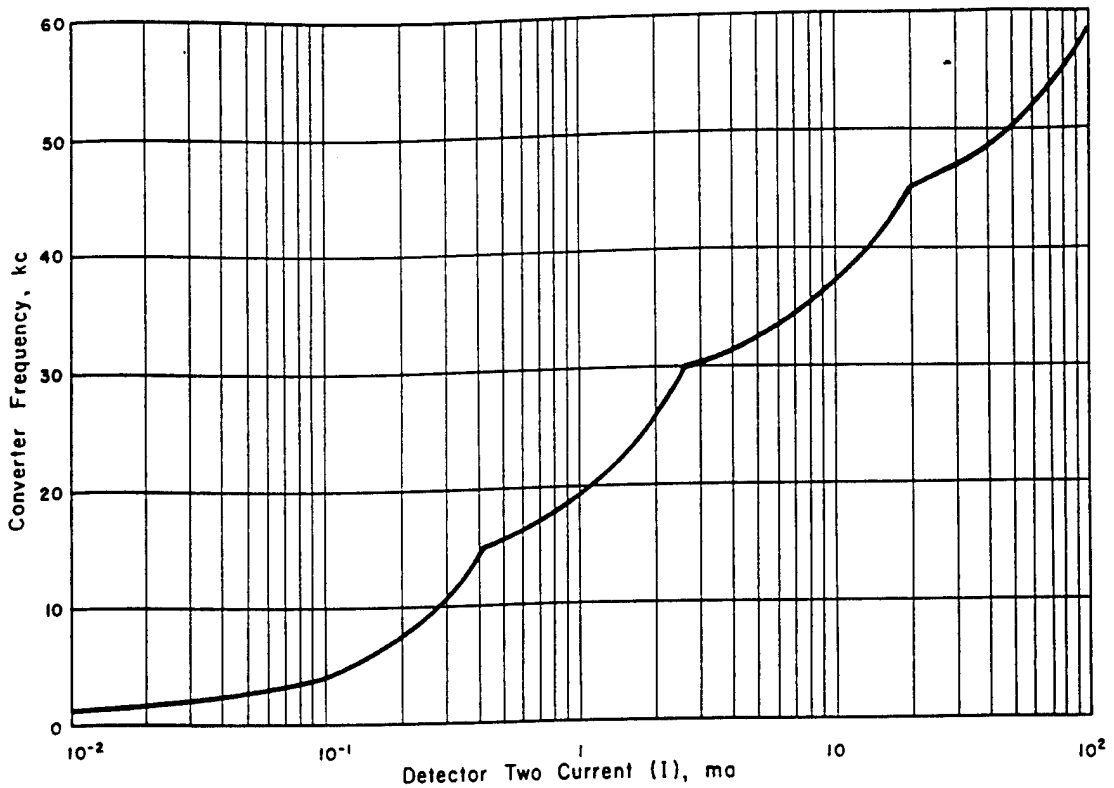

Figure 2.13 Detector 2, $Li^{6}I$, channel calibration curve.

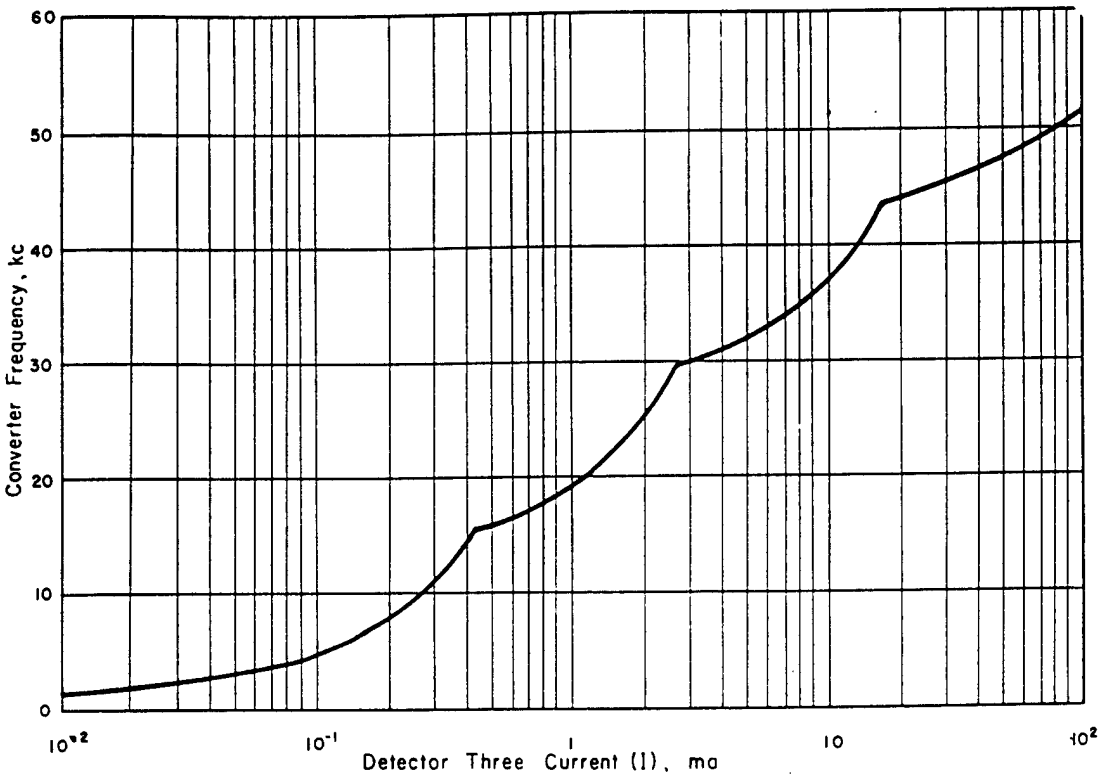

Figure 2.14 Detector 3, LiI, channel calibration curve.

recorder to record for 120 msec and then to be locked into the playback mode for the duration of the life of the canister

Provisions were made to supply external power and simulate the commands for pre-flight testing and calibration. In-flight power was supplied by Yardney Silver-Cells.

2.6 GROUND STATION

The ground station was designed primarily for Project 1.10 functions (Reference 4), but was entirely adequate for the purposes of Project 2.7. During the playback period of the Project 2.7 tape recorder, the telemeter receiver outputs were simultaneously

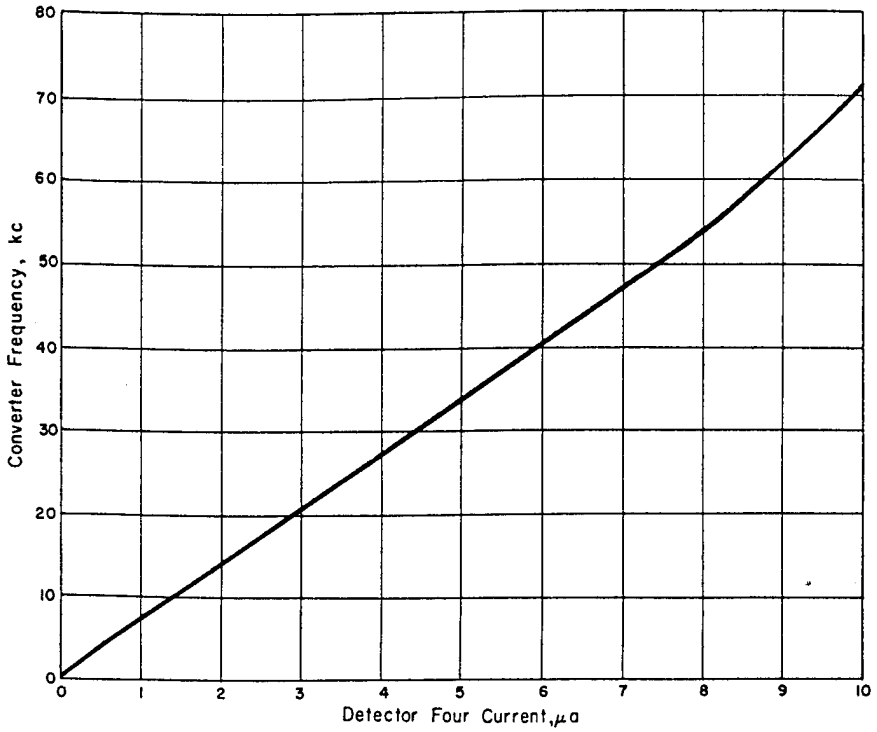

Figure 2.15 Detector 4, KBr, channel calibration curve.

recorded on an Ampex 800 tape recorder and run through a discriminator array into a consolidated recording oscillograph. The oscillograph record provided a quick look at the data and the tape record was available for detailed processing of the data.

2.7 FORM AND ACCURACY OF DATA

With the exception of the initial rise of the neutron pulse, the data was to have been obtained as a series of pulses of variable spacing on the tape from the Ampex 800 in the ground station. This would have been transcribed to film by deflection of an oscilloscope trace with the output of the tape recorder and photographing the trace with a moving-film camera. The pulse frequency could then be determined as a function of time, the electronic calibration curves could be used to find detector outputs, and the procedure outlined in Section 1.3 finally used to obtain the neutron source function. It would be possible to make an electronic pulse counter of sufficiently fast response to have graphed the pulse

spacing automatically, but the method outlined above is considered inherently more accurate.

The leading edge of the neutron pulse could also be transcribed to film. Here, the transient response of the canister system is very important, and studies of this are not complete. However, it should be possible to determine a reasonable equivalent transfer function for use in obtaining the detector-current function giving rise to this output pulse. This procedure will give only the shape of the leading edge of the pulse. The amplitude must be determined from the pulse rate at the time the system reverts to converter recording. This difficulty arises from the inability of tape recorders to faithfully reproduce amplitude recorded information. Consecutive recorded pulses may vary as much as a factor of four in amplitude, although the average amplitude should remain accurate to about 5 percent.

The accuracy possible with the system should be of the order of ± 25 percent for the converter information at low frequencies, increasing with frequency. It was expected that neutron-pulse-rise information would have been worse than this and would not have been capable of evaluation until the transfer function investigation had been completed.

Chapter 3
RESULTS and DISCUSSION

No data was obtained. The Project 1.10 command system failed at minus 2:15 minutes, and Commands 2, 3, and 4 were not transmitted. This left the Project 2.7 canister in the unarmed condition at zero time. Although the data was probably recorded, the system did not lock into the playback mode, so the data was erased on the next transit of the tape loop. It was apparent from the ground station recordings that the Project 2.7 instrumentation was operating properly in the "ready" condition, both before and after zero time, since the idling rates of the converters were present. Only about 6 percent of the data would have been obtained in any event, because the Project 1.10 telemeter transmitter in Canister 5 failed at plus 2.5 seconds.

The records of field strength made by the ground station may yield some information on the blackout effect at these altitudes. Canister 2, at 1,050 feet from the burst began to recover in about 3.9 seconds; and Canister 5, at 2,750 feet, began to recover in about 0.08 second.

Chapter 4
CONCLUSIONS and RECOMMENDATIONS

4.1 CONCLUSIONS

The balloon system left nothing to be desired in ease of launching and getting instrumentation of this type to altitude. The difficulties encountered with the command and telemetering systems could certainly be corrected by adequate testing in an environment including nuclear radiation of the intensity encountered here. The technique used seems well suited for tests in the 100,000-foot-altitude range and, if repeated with thoroughly tested systems, should offer an excellent chance of success.

4.2 RECOMMENDATIONS

The Project 2.7 instrumentation performed satisfactorily, in view of the circumstances; but if the experiment should be repeated, the instrumentation should be tested on the ground in a nuclear-radiation environment.

REFERENCES

1. T. D. Hanscome and D. K. Willett; "Neutron Flux Measurements"; Project 2.2, Operation Teapot, WT–1116; Naval Research Laboratory, Washington, D. C.; Secret Restricted Data.

2. P. A. Caldwell and others; "Attenuation of High Frequency and Ultra High Frequency by Ionization Resulting From Nuclear Explosions"; Project 6.6, Operation Redwing, ITR–1346, July 1956; Naval Research Laboratory, Washington, D. C.; Secret Restricted Data.

3. T. D. Hanscome and others; "Parameters Affecting Design of Instrumentation to Measure Gamma and Neutron Fluxes from a Very-High-Altitude Nuclear Detonation"; Project 2.7, Operation Plumbbob, ITR–1416; Naval Research Laboratory, Washington, D. C.; Secret Restricted Data.

4. N. A. Haskell and J. T. Pantall; "Blast Overpressure from Very-High-Altitude Bursts"; Project 1.10, Operation Hardtack, ITR–1615; Air Force Cambridge Research Center, Bedford, Massachusetts; Secret Restricted Data.

DISTRIBUTION

Military Distribution Category 5-80

ARMY ACTIVITIES

1 Asst. Dep. Chief of Staff for Military Operations, D/A, Washington 25, D.C. ATTN: Asst. Executive (R&SW)
2 Chief of Research and Development, D/A, Washington 25, D.C. ATTN: Atomic Division
3 Chief of Ordnance, D/A, Washington 25, D.C. ATTN: ORDTX-AR
4 Chief Signal Officer, D/A, P&O Division, Washington 25, D.C. ATTN: SIGRD-8
5 The Surgeon General, D/A, Washington 25, D.C. ATTN: MEDNE
6- 7 Chief Chemical Officer, D/A, Washington 25, D.C.
8 The Quartermaster General, D/A, Washington 25, D.C. ATTN: Research and Development
9- 11 Chief of Engineers, D/A, Washington 25, D.C. ATTN: ENGNB
12 Chief of Transportation, Military Planning and Intelligence Div., Washington 25, D.C.
13- 15 Commanding General, Headquarters, U. S. Continental Army Command, Ft. Monroe, Va.
16 President, Board #1, Headquarters, Continental Army Command, Ft. Sill, Okla.
17 President, Board #2, Headquarters, Continental Army Command, Ft. Knox, Ky.
18 President, Board #4, Headquarters, Continental Army Command, Ft. Bliss, Tex.
19 Commanding General, Headquarters, First U. S. Army, Governor's Island, New York 4, N.Y.
20 Commanding General, Headquarters, Second U. S. Army, Ft. George G. Meade, Md.
21 Commanding General, Headquarters, Third U. S. Army, Ft. McPherson, Ga. ATTN: ACofS, G-3
22 Commanding General, Headquarters, Fourth U. S. Army, Ft. Sam Houston, Tex. ATTN: G-3 Section
23 Commanding General, Headquarters, Fifth U. S. Army, 1660 E. Hyde Park Blvd., Chicago 15, Ill.
24 Commanding General, Headquarters, Sixth U. S. Army, Presidio of San Francisco, San Francisco, Calif. ATTN: AMGCT-4
25 Commanding General, U.S. Army Caribbean, Ft. Amador, C.Z. ATTN: Cml. Off.
26 Commanding General, USARFANT & MDPR, Ft. Brooke, Puerto Rico
27 Commanding General, Southern European Task Force, APO 168, New York, N.Y. ATTN: ACofS, G-3
28 Commanding General, Eighth U.S. Army, APO 301, San Francisco, Calif. ATTN: ACofS, G-3
29 Commanding General, U.S. Army Alaska, APO 942, Seattle, Wash.
30- 31 Commanding General, U.S. Army Europe, APO 403, New York, N.Y. ATTN: OPOT Div., Combat Dev. Br.
32- 33 Commandant, Command and General Staff College, Ft. Leavenworth, Kan. ATTN: ALLLS(AS)
34 Commandant, The Artillery and Missile School, Ft. Sill, Okla.
35 Secretary, The U.S. Army Air Defense School, Ft. Bliss, Texas. ATTN: Maj. Ergan V. Roth, Dept. of Tactics and Combined Arms
36 Commanding General, Army Medical Service School, Brooke Army Medical Center, Ft. Sam Houston, Tex.
37 Director, Special Weapons Development Office, Headquarters, CONARC, Ft. Bliss, Tex. ATTN: Capt. T. E. Skinner
38 Superintendent, U.S. Military Academy, West Point, N. Y. ATTN: Prof. of Ordnance
39 Commandant, Chemical Corps School, Chemical Corps Training Command, Ft. McClellan, Ala.
40- 41 Commanding General, U.S. Army Chemical Corps, Research and Development Command, Washington, D.C.
42 Commanding General, Aberdeen Proving Grounds, Md. ATTN: Director, Ballistics Research Laboratory
43 Commanding General, The Engineer Center, Ft. Belvoir, Va. ATTN: Asst. Commandant, Engineer School
44 Commanding Officer, Engineer Research and Development Laboratory, Ft. Belvoir, Va. ATTN: Chief, Technical Intelligence Branch
45 Commanding Officer, Picatinny Arsenal, Dover, N.J. ATTN: ORDBB-TK
46 Commanding Officer, Frankford Arsenal, Philadelphia 37, Pa. ATTN: Col. Tewes Kundel
47- 48 Commanding Officer, Chemical Warfare Laboratories, Army Chemical Center, Md. ATTN: Tech. Library
49 Commanding Officer, Transportation R&D Station, Ft. Eustis, Va.
50 Commandant, The Transportation School, Ft. Eustis, Va. ATTN: Security and Information Officer
51 Operations Research Office, Johns Hopkins University, 6935 Arlington Rd., Bethesda 14, Md.
52- 54 Commanding General, Quartermaster Research and Development, Command, Quartermaster Research and Development Center, Natick, Mass. ATTN: CBR Liaison Officer
55 Commanding General, Quartermaster Research and Engineering Command U.S. Army, Natick, Mass.
56- 60 Technical Information Service Extension, Oak Ridge, Tenn.

NAVY ACTIVITIES

61- 62 Chief of Naval Operations, D/N, Washington 25, D. C. ATTN: OP-36
63 Chief of Naval Operations, D/N, Washington 25, D.C. ATTN: OP-03EG
64 Chief, Bureau of Medicine and Surgery, D/N, Washington 25, D.C. ATTN: Special Weapons Defense Div.
65 Chief, Bureau of Ordnance, D/N, Washington 25, D.C.
66 Chief of Naval Personnel, D/N, Washington 25, D.C.
67 Chief, Bureau of Ships, D/N, Washington 25, D.C. ATTN: Code 348
68 Chief, Bureau of Supplies and Accounts, D/N, Washington 25, D.C.
69- 70 Chief, Bureau of Aeronautics, D/N, Washington 25, D.C.
71 Chief of Naval Research, Department of the Navy Washington 25, D.C. ATTN: Code 811
72 Commander-in-Chief, U.S. Atlantic Fleet, U.S. Naval Base, Norfolk 11, Va.
73 Commandant, U.S. Marine Corps, Washington 25, D.C. ATTN: Code A03H
74 Superintendent, U.S. Naval Postgraduate School, Monterey, Calif.
75 Commander, Joint Task Force Seven, Arlington Hall Station, Arlington 12, Va., ATTN: TS and RD
76 Commanding Officer, U.S. Naval Schools Command, U.S. Naval Station, Treasure Island, San Francisco, Calif.
77 Commanding Officer, U.S. Fleet Training Center, Naval Base, Norfolk 11, Va. ATTN: Special Weapons School
78 Special Weapons Unit, Pacific, U. S. Naval Air Station, North Island, San Diego 35, Calif.
79 Commanding Officer, U.S. Naval Damage Control Training Center, Naval Base, Philadelphia, Pa. ATTN: ABC Defense Course
80 Commander, U.S. Naval Ordnance Laboratory, Silver Spring 19, Md. ATTN: R
81 Commander, U.S. Naval Ordnance Test Station, Inyokern, China Lake, Calif.
82 Officer-in-Charge, U.S. Naval Civil Engineering Res. and Evaluation Lab., U.S. Naval Construction Battalion Center, Port Hueneme, Calif. ATTN: Code 753
83 Commanding Officer, U.S. Naval Medical Research Inst., National Naval Medical Center, Bethesda 14, Md.

[redacted]

84 Director, U.S. Naval Research Laboratory, Washington 25, D.C. ATTN: Mrs. Katherine H. Cass
85 Director, The Material Laboratory, New York Naval Shipyard, Brooklyn, N. Y.
86 Commanding Officer and Director, U.S. Navy Electronics Laboratory, San Diego 52, Calif. ATTN: Code 4223
87- 88 Commanding Officer, U.S. Naval Radiological Defense Laboratory, San Francisco, Calif. ATTN: Technical Information Division
89 Commanding Officer and Director, David W. Taylor Model Basin, Washington 7, D.C. ATTN: Library
90 Commander, U.S. Naval Air Development Center, Johnsville, Pa.
91 Commander-in-Chief Pacific, Pearl Harbor, TH
92 Commander, Norfolk Naval Shipyard, Portsmouth 8, Va. ATTN: Code 270
93- 98 Technical Information Service Extension, Oak Ridge, Tenn. (Surplus)

AIR FORCE ACTIVITIES

99 Asst. for Atomic Energy Headquarters, USAF, Washington 25, D.C. ATTN: DCS/O
100 Director of Operations, Headquarters, USAF, Washington 25, D.C. ATTN: Operations Analysis
101 Director of Plans, Headquarters, USAF, Washington 25, D.C. ATTN: War Plans Div.
102 Director of Research and Development, DCS/D, Headquarters, USAF, Washington 25, D.C. ATTN: Combat Components Div.
103-104 Director of Intelligence, Headquarters, USAF, Washington 25, D.C. ATTN: AFOIN-IB2
105 The Surgeon General, Headquarters, USAF, Washington 25, D.C. ATTN: Bio. Def. Br., Pre. Med. Div.
106 Asst. Chief of Staff, Intelligence, Headquarters, U.S. Air Forces-Europe, APO 633, New York, N.Y. ATTN: Directorate of Air Targets
107 Commander, 497th Reconnaissance Technical Squadron (Augmented), APO 633, New York, N.Y.
108 Commander-in-Chief, Pacific Air Forces, APO 953, San Francisco, Calif., ATTN: PFCIE-MB, Base Recovery
109 Commander-in-Chief, Strategic Air Command, Offutt AFB, Omaha, Nebraska. ATTN: OAWS
110 Commander, Tactical Air Command, Langley AFB, Va. ATTN: Documents Security Branch
111 Commander, Air Defense Command, Ent AFB, Colo.
112 Commander, Air Materiel Command, Wright-Patterson AFB, Dayton, Ohio. ATTN: MCSW
113 Commander, Air Research and Development Command, Andrews AFB, Washington 25, D.C. ATTN: RDDN
114 Commander, Air Proving Ground Command, Eglin AFB, Fla. ATTN: Adj./Tech. Report Branch
115-116 Director, Air University Library, Maxwell AFB, Ala.
117-122 Commander, Air Training Command, Randolph AFB, Tex.
123-124 Commandant, Air Force School of Aviation Medicine, Randolph AFB, Tex.
125 Commander, Wright Air Development Center, Wright-Patterson AFB, Dayton, Ohio. ATTN: WCOSI
126-127 Commander, Air Force Cambridge Research Center, LG Hanscom Field, Bedford, Mass. ATTN: CRQST-2
128-130 Commander, Air Force Special Weapons Command, Kirtland AFB, N. Mex. ATTN: Tech. Information Office
131 Commander, Lowry AFB, Denver, Colo. ATTN: Department of Special Weapons Training
132 Commander, 1009th Special Weapons Squadron, Headquarters, USAF, Washington 25, D.C.
133-134 The RAND Corporation, 1700 Main Street, Santa Monica, Calif. ATTN: Nuclear Energy Division
135 Commander, Western Development Div. (ARDC), PO Box 262, Inglewood, Calif. ATTN: WDSIT, R. G. Weitz
136-140 Technical Information Service Extension, Oak Ridge, Tenn. (Surplus)

OTHER DEPARTMENT OF DEFENSE ACTIVITIES

141 Asst. Secretary of Defense, Research and Engineering, D/D, Washington 25, D.C. ATTN: Tech. Library
142 U.S. Documents Officer, Office of the U.S. National Military Representative, SHAPE, APO 55, New York, N.Y.
143 Director, Weapons Systems Evaluation Group, OSD, Rm 2E1006, Pentagon, Washington 25, D.C.
144 Chairman, Armed Services Explosives Safety Board, D/D, Building T-7, Gravelly Point, Washington 25, D.C.
145 Commandant, Armed Forces Staff College, Norfolk 11, Va. ATTN: Secretary
146 Commander, Field Command, Armed Forces Special Weapons Project, PO Box 5100, Albuquerque, N. Mex.
147 Commander, Field Command, Armed Forces Special Weapons Project, PO Box 5100, Albuquerque, N. Mex. ATTN: Technical Training Group
148-152 Commander, Field Command, Armed Forces Special Weapons Project, P.O. Box 5100, Albuquerque, N. Mex. ATTN: Deputy Chief of Staff, Weapons Effects Test
153-163 Chief, Armed Forces Special Weapons Project, Washington 25, D.C. ATTN: Documents Library Branch
164 Commanding General, Military District of Washington, Room 1543, Building T-7, Gravelly Point, Va.
165-169 Technical Information Service Extension, Oak Ridge, Tenn. (Surplus)

ATOMIC ENERGY COMMISSION ACTIVITIES

170-172 U.S. Atomic Energy Commission, Classified Technical Library, Washington 25, D.C. ATTN: Mrs. J. M. O'Leary (For DMA)
173-174 Los Alamos Scientific Laboratory, Report Library, PO Box 1663, Los Alamos, N. Mex. ATTN: Helen Redman
175-179 Sandia Corporation, Classified Document Division, Sandia Base, Albuquerque, N. Mex. ATTN: H. J. Smyth, Jr.
180-182 University of California Radiation Laboratory, PO Box 808, Livermore, Calif. ATTN: Clovis G. Craig
183 Weapon Data Section, Technical Information Service Extension, Oak Ridge, Tenn.
184-190 Technical Information Service Extension, Oak Ridge, Tenn. (Surplus)

[redacted]